






# Microbial diversity through an oceanographic lens: refining the concept of ocean provinces through trophic-level analysis and productivity-specific length scales

Cora Hörstmann <sup>1,2\*</sup> Pier Luigi Buttigieg <sup>3</sup>  
Uwe John <sup>1,4</sup> Eric J. Raes <sup>5</sup> Dieter Wolf-Gladrow,<sup>1</sup>  
Astrid Bracher <sup>1,6</sup> and Anya M. Waite <sup>5</sup>

<sup>1</sup>Alfred Wegener Institute Helmholtz Center for Polar and Marine Science, Bremerhaven, Germany.

<sup>2</sup>Department of Life Sciences and Chemistry, Jacobs University gGmbH, Bremen, Germany.

<sup>3</sup>Helmholtz Metadata Collaboration, GEOMAR, Kiel, Germany.

<sup>4</sup>Helmholtz Institute for Functional Marine Biodiversity, Oldenburg, Germany.

<sup>5</sup>Ocean Frontier Institute and Department of Oceanography, Dalhousie University, Halifax, NS, Canada.

<sup>6</sup>Institute of Environmental Physics, University of Bremen, Bremen, Germany.

## Summary

**In the marine realm, microorganisms are responsible for the bulk of primary production, thereby sustaining marine life across all trophic levels. Longhurst provinces have distinct microbial fingerprints; however, little is known about how microbial diversity and primary productivity change at finer spatial scales. Here, we sampled the Atlantic Ocean from south to north (~50°S–50°N), every ~0.5° latitude. We conducted measurements of primary productivity, chlorophyll-*a* and relative abundance of 16S and 18S rRNA genes, alongside analyses of the physicochemical and hydrographic environment. We analysed the diversity of autotrophs, mixotrophs and heterotrophs, and noted distinct patterns among these guilds across provinces with high and low chlorophyll-*a* conditions. Eukaryotic autotrophs and prokaryotic heterotrophs showed a shared inter-province diversity pattern, distinct from the diversity**

**pattern shared by mixotrophs, cyanobacteria and eukaryotic heterotrophs. Additionally, we calculated samplewise productivity-specific length scales, the potential horizontal displacement of microbial communities by surface currents to an intrinsic biological rate (here, specific primary productivity). This scale provides key context for our trophically disaggregated diversity analysis that we could relate to underlying oceanographic features. We integrate this element to provide more nuanced insights into the mosaic-like nature of microbial provincialism, linking diversity patterns to oceanographic transport through primary production.**

## Introduction

The continuous movement of seawater and turnover of microbial biomass and diversity in marine ecosystems form a time-varying mosaic of phylogenetic and functional biodiversity across ocean basins. This complicates efforts to map, understand and monitor key marine ecosystem attributes such as microbial growth, biodiversity and carbon cycling (Stec *et al.*, 2017).

Marine ecosystems comprise a wide array of microbial life: microbial (photo-)autotrophic, pro- and eukaryotes, form the base of the marine food web (Hutchins *et al.*, 2015; Sunagawa *et al.*, 2015), and sustain energy exchange, provision and recycling of resources (Falkowski *et al.*, 2008; Guidi *et al.*, 2016) for higher trophic levels. Heterotrophs and mixotrophs remineralize most of the carbon and nutrients from the primary production via the microbial loop, before these can be exported to the deep sea (Azam *et al.*, 1983; Azam and Malfatti, 2007).

In terrestrial systems, primary producer communities have been used to define major biomes (Woodward, 1987; Woodward *et al.*, 2004), biogeographic realms and ecoregions (Olson *et al.*, 2001) through their physical and functional structuring of ecosystems (Cardinale *et al.*, 2011). In the ocean, Longhurst (2007) used chlorophyll-*a* (chl *a*) concentrations as a proxy for

Received 3 March, 2021; revised 28 October, 2021; accepted 28 October, 2021. \*For correspondence. E-mail cora.hoerstmann@awi.de; Fax +49(471)4831-1149; Tel. +49(471)4831-1496.

phytoplankton biomass to delimit ocean provinces, alongside water temperature to distinguish water masses. Longhurst provinces are used to define oceanographic biogeographic subdivisions; however, static applications of these provinces typically overlook the dynamic interactions, life histories, endemism and/or vicariance within ecological assemblages, needed to truly map microbial biogeography. Thus, multiple variables including biomass, primary productivity (PP), and diversity need to be considered with carefully structured sampling across space and time (Kollmann *et al.*, 2016). Here, we investigate how integrating multiple physical and biochemical variables – accounting for their horizontal displacement by surface currents – can improve our understanding of microbial provincialization across a high-resolution transect ( $\sim 0.5^\circ$  latitude) of the Atlantic Ocean.

Microbial assemblages can act as ‘fingerprints’ for water masses thanks to their high diversity, responsiveness and (typically) fast generation time (hours to days; Martiny *et al.*, 2006), aiding the definition of biogeographic boundaries in pelagic environments (Raes *et al.*, 2011; Fuhrman *et al.*, 2015). However, the dynamic nature of the oceans – with their fronts, currents, eddies, up- and downwellings, and other hydrographic features – has the potential to add additional complexity to the ecological variation between and within such regions (Oliver and Irwin, 2008; Hernando-Morales *et al.*, 2017).

Hydrographic features create structural variability in the ocean, which (through, e.g. modifying nutrient distributions) provides more diverse niche space for microbial communities to colonize. Unless mitigated, this would increase microbial diversity (e.g. Kemp and Mitsch, 1979; Cadotte, 2006) and should favour phytoplankton productivity (Legendre, 1981). While basin-scale horizontal dispersal of organisms by major ocean currents is known to reduce microbial  $\beta$ -diversity (Raes *et al.*, 2011; Richter *et al.*, 2020; Sommeria-Klein *et al.*, 2021), mesoscale and sub-mesoscale horizontal transport of microbial communities, and the impact on their activity, is rarely taken into account, except in a few frameworks that couple ecology and hydrography (e.g. the ‘dual-lens’ approach; Oldham *et al.*, 2013). Indeed, hydrographic dynamics within and between ocean provinces interact with both neutral and selective ecological processes, resulting in communities in different successional states (Zhou *et al.*, 2014) and/or shaped by opportunistic responses (e.g. Duffy and Stachowicz, 2006; Hartmann *et al.*, 2012; Fadeev *et al.*, 2021).

Here, we assess the relative importance of regional water mass characteristics (physicochemical parameters and hydrography) on microbial diversity. Furthermore, we resolve diversity responses along major trophic groups (auto-, mixo-, heterotrophs), an important but understudied perspective in microbial ecology (reviewed in

Seibold *et al.*, 2018). We leverage a conceptual framework that asserts that microbial communities are distinct within oceanographic regions, separated by fronts and currents limiting microbial dispersal (Martiny *et al.*, 2006; Milici *et al.*, 2016; Raes *et al.*, 2018). We then assess how ecosystem structure (i.e. hydrography), bottom-up and top-down factors can qualify and advance traditional partitioning of the Atlantic into biogeographic provinces.

## Results

### *Delineation of oceanographic, ecosystemic provinces*

Our analyses of remote sensing observations of geostrophic currents, sea surface temperature and chl *a* combined with *in situ* measurements of oceanographic features, chl *a* and microbial diversity informed our determination of ecosystem boundaries shown in Fig. 1. The ecosystem boundaries broadly overlapped with the Longhurst Provinces and we thus maintain the same naming conventions (Fig. S1). One exception was the South Atlantic Gyral (SATL) province, wherein sites were clearly ordinated into separate groups; one with cool waters (COLD;  $20.4\text{--}23.3^\circ\text{C}$ ) in the Argentine Basin, south of the Rio Grande rise and northern, oligotrophic warmer waters (HOT;  $25.1\text{--}27.5^\circ\text{C}$ ) in the Brazil Basin (Figs S2 and S3). Furthermore, Stations 24 and 92 were outliers with respect to the temperature-salinity plot used for identifying ecosystem boundaries (Fig. S2), and were thus not grouped in an ocean province.

On a broad scale, we could separate ocean provinces into provinces with low and high chl *a* with significant differences in chl *a* concentrations (Wilcoxon,  $p$ -value =  $9.112\text{e}^{-6}$ ,  $n_1 = 38$ ,  $n_2 = 39$ ), and significant differences in PP (Wilcoxon,  $p$ -value =  $3.686\text{e}^{-5}$ ,  $n_1 = 38$ ,  $n_2 = 39$ ; Table 1). In our principal component analysis (PCA) (Fig. S4), sites in the Southwest Atlantic Shelves province (FKLD), Brazil Current Coast province (BRAZ), Canary Current Coast province (CNRy), North Atlantic Subtropical Gyre province (NAST-E) and North Atlantic Drift province (NADR) (i.e. high-chl *a*) provinces were associated with high particulate organic matter and high dissolved inorganic nutrient concentrations. Furthermore, the SATL-COLD, SATL-HOT, Western Tropical Atlantic province (WTRA) and North Atlantic Tropical Gyre province (NATR) (i.e. low-chl *a* provinces) provinces were associated with low temperatures and larger distance to coast ( $>600$  km; Fig. S4).

Province PP and chl *a* concentrations correlate across the transect (Pearson correlation;  $r = 0.48$ ,  $p = 6.68\text{e}^{-6}$ ,  $n = 80$ ), but did not always correlate within provinces (e.g. WTRA:  $r = 0.08$ ,  $p = 0.8$ ,  $n = 11$ ). We measured the highest PP in the CNRY province, a peak in chl *a* concentrations relative to adjacent ocean provinces

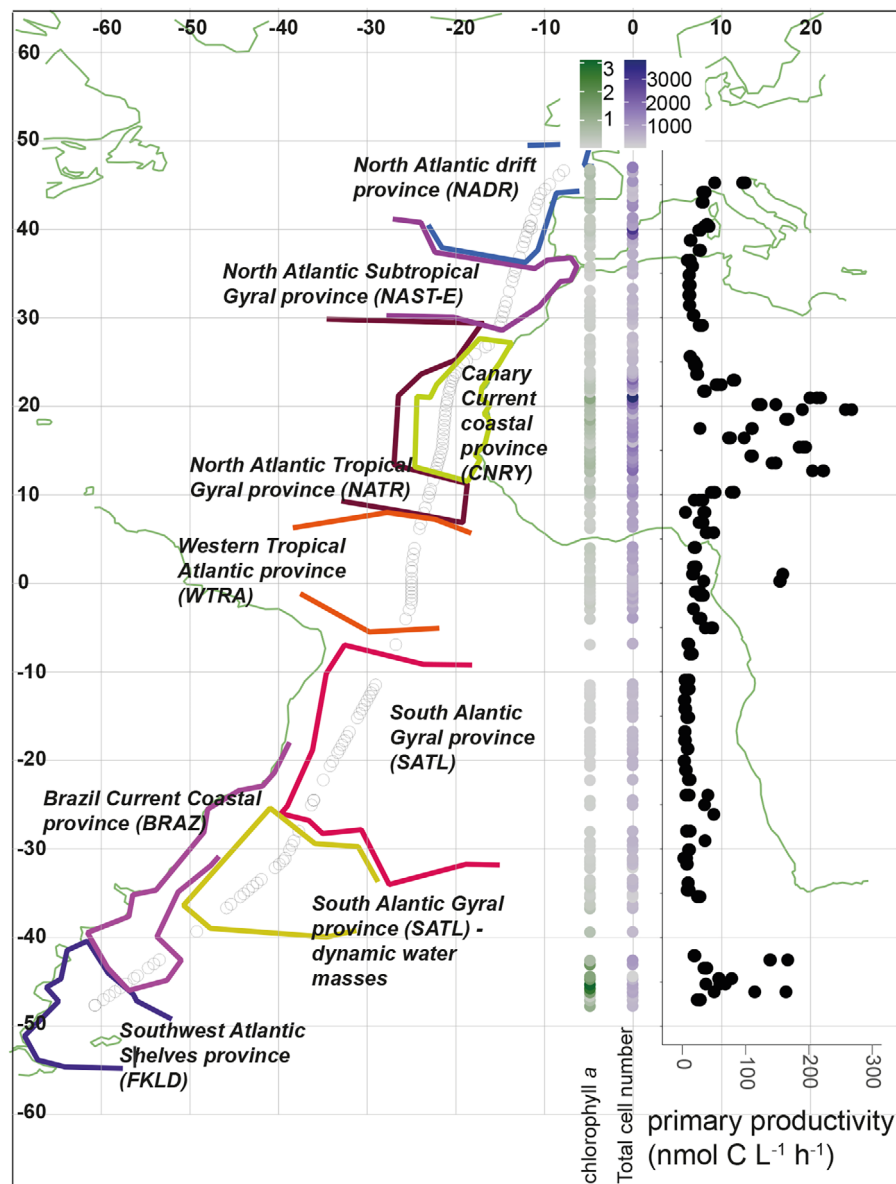


**Fig. 1.** Map of the PS113 expedition showing chl *a* concentration gradients ranging from 0 to 3 mg chl *a* m<sup>-3</sup>, total nanoplanktonic cell number (ranging from 1000 to 3000 cells μl<sup>-1</sup>) and primary productivity (PP) (nmol C L<sup>-1</sup> h<sup>-1</sup>) against latitude. Stations are indicated by circles. Ocean provinces are indicated with coloured lines.

(Table 1), and total cell numbers of  $1207 \pm 737$  cells μl<sup>-1</sup> (mean  $\pm$  SD,  $n = 30$ ; Table S1).

#### Biomass turnover and transport of pelagic microbial communities

In the following analyses, we used a quantitative comparison of biomass turnover (specific PP;  $P^B$ ) and current speed (see Methods, Eqs. 3 and 4) to estimate the distance a microbial community has travelled through passive advection before half of its biomass has been turned over: the productivity-specific length scale (Fig. 2A).

Based on the biological and physical component of the productivity-specific length scale, we observed strong

sample variations in both variables [ $P^B$  based on PP per day (d) and chl *a*, Table 1, and surface current speed] within and between provinces (Fig. 2B). For example, the SATL-HOT province had high variations in  $P^B$  (0.007–0.07 mg C m<sup>-3</sup> d<sup>-1</sup>,  $n = 15$ ) with relatively constant horizontal current speed (1–3 m d<sup>-1</sup>). In contrast, we measured a large range of horizontal current speed (2–7 m d<sup>-1</sup>,  $n = 4$ ) at relatively low  $P^B$  (0.002–0.01 mg C m<sup>-3</sup> d<sup>-1</sup>,  $n = 4$ ) within the BRAZ province resulting in the largest productivity-specific length scales (up to 22 km) of our dataset.

We used our calculations of sample-specific productivity-specific length scales to examine variabilities in beta diversity ( $\beta$ -diversity) between neighbouring sites

**Table 1.** Physico-chemical properties, primary productivity, chl *a* concentrations and productivity-specific length scale of ocean provinces during the PS113 expedition. Provinces are separated into high-chl *a* provinces and low-chl *a* provinces.

Province	H-CHL/ L-CHL	Temperature	Salinity	POC (nM)	PN (nM)	Nitrate ( $\mu\text{M}$ )	Phosphate ( $\mu\text{M}$ )	PP (nmol C L <sup>-1</sup> h <sup>-1</sup> )			chl <i>a</i> (mg m <sup>-3</sup> )			n	PL	n
								Range	Mean $\pm$ SD	Range	Mean $\pm$ SD	Range	Mean $\pm$ SD			
BRAZ	H-CHL	11.26–18.62	33.98–35.28	4071–16 953	608–2913	0.43–2.43	0.36–0.55	36.7–108.1	65.77	0.81–3.1	1.78	0.81–3.1	1.78	4	3.5–22.6	4
Station 24	H-CHL	19.89	36.14	3070	488.5	8.9	0.71	146	146	0.72		0.72		1	2.2	1
CNRY	H-CHL	19.96–22.58	35.87–37.05	3201–24 922	250.1–4371.3	0–3.8	0.01–0.31	12.8–234.7	105.82 $\pm$ 75	0.13–1.22	0.49 $\pm$ 0.3	0.13–1.22	0.49 $\pm$ 0.3	17	0.4–3.2	17
FKLD	H-CHL	8.19–9.42	33.76–33.99	4459–8246	497–1474	13.095	1.08	26.41	26.41	0.65	0.65	0.65	0.65	1	4.4	1
NADR	H-CHL	15.32–17.07	35.55–35.92	4904–12 717	466.5–1875.9	0.01	0.04–0.08	13.3–81	36.6 $\pm$ 20	0.14–0.44	0.32 $\pm$ 0.1	0.14–0.44	0.32 $\pm$ 0.1	8	0.6–4.5	8
NAST-E	H-CHL	17.55–25.14	36.14–36.93	2948–5731	227.2–779.8	<0.01	0.01–0.09	11.1–29.1	15.00 $\pm$ 6	0.07–0.18	0.13 $\pm$ 0.0	0.07–0.18	0.13 $\pm$ 0.0	8	0.9–6.9	8
NATR	H-CHL	23.98–26.12	35.95–36.13	5356–9138	670.1–1237.8	0.01–0.3	0.02–0.19	24.9–79.3	44.76	0.14–0.43	0.3	0.14–0.43	0.3	4	0.8–1.8	4
SATL-COLD	L-CHL	20.39–23.28	35.83–36.30	2188–4357	257.9–561.6	<0.11	<0.1	4.7–35.7	14.63 $\pm$ 10	0.08–0.32	0.18 $\pm$ 0.1	0.08–0.32	0.18 $\pm$ 0.1	9	1.2–12.2	9
SATL-HOT	L-CHL	25.14–27.54	36.93–37.41	1525–3042	58.2–377.3	<0.04	<0.1	3.6–49.3	12.3 $\pm$ 13	0.04–0.13	0.07 $\pm$ 0.0	0.04–0.13	0.07 $\pm$ 0.0	15	0.4–4.7	15
WTRA	L-CHL	27.32–28.65	34.16–36.27	2609–4455	265.4–594.9	<0.2	<0.09	17.8–112.7	39.25 $\pm$ 28	0.13–0.35	0.21 $\pm$ 0.1	0.13–0.35	0.21 $\pm$ 0.1	11	0.7–9.2	11
Station 90 + 92	L-CHL	28.33	36.33	2703	296.6	0.01	0.02–0.07	9.7–13.6	12.67	0.09–0.1	0.09	0.09–0.1	0.09	2	1.4–2.1	2

(Fig. 2C). We noted three major regimes in our joint analysis of  $\beta$ -diversity and productivity-specific length scales (Fig. 2C): The first regime matches the CNRY province and shows markedly high variability in  $\beta$ -diversity but always at low (<5 km) productivity-specific length scales. The second regime shows a largely random scatter bounded by a well-defined upper threshold of  $\beta$ -diversity (0.05 ordination distance). Similar to the first regime, we observed this distribution of  $\beta$ -diversity to be restricted to productivity-specific length scales under 5 km. The final regime occurs at productivity-specific length scales between 5 and 18 km. We observed an increase in  $\beta$ -diversity with increasing productivity-specific length scales. However, the variation between functional trophic groups increased with increasing productivity-specific length scales, too. Cyanobacteria, eukaryotic heterotrophs and mixotrophs were more similar to each other with a stronger increase in  $\beta$ -diversity compared to the  $\beta$ -diversity observed in prokaryotic heterotrophs and eukaryotic autotrophs.

#### Alpha diversity ( $\alpha$ -diversity) across functional groups and oceanographic provinces

Rarefaction curves for both prokaryotes and eukaryotes saturated in all samples (Fig. S5). Prokaryotic Shannon diversity was highest (260.1) at Station 11 (BRAZ province) and lowest (59) at Station 97 (WTRA province; Table S2). Eukaryotic Shannon diversity was highest (766.8) at Station 45 (SATL-COLD province) and lowest (11.2) at Station 8 (BRAZ province; Table S2).

We observed that  $\alpha$ -diversity varied across trophic groups, provinces and latitude (Fig. 3A). The  $\alpha$ -diversity of both eukaryotic and prokaryotic autotrophs and eukaryotic mixotrophs was lower than that of heterotrophs. Relative to other functional groups, heterotrophic prokaryotes had higher  $\alpha$ -diversity in the southernmost and northernmost provinces (FKLD, BRAZ, NADR). Shannon diversity increased towards the equator and was most pronounced for heterotrophic pro- and eukaryotes (Fig. 3A) with the highest  $\alpha$ -diversity in the SATL-HOT, SATL-COLD and WTRA provinces (Table S2); the warmest and most oligotrophic provinces sampled. Similarly, the low-chl *a* provinces had significantly higher mixotrophic  $\alpha$ -diversity than the high-chl *a* provinces (Wilcoxon,  $p < 2.2e^{-16}$ ,  $n_1 = 39$ ,  $n_2 = 68$ ).

In relation to the physical-chemical parameters,  $\alpha$ -diversity was positively and linearly correlated with physical variables (temperature and salinity), and negatively correlated with nutrient and biochemical concentrations ( $\text{NO}_3$ ,  $\text{PO}_4$ , POC, PN, chl *a*) across ocean provinces (Fig. 3B). The correlation between temperature and  $\alpha$ -diversity was significant for autotrophic eukaryotes, mixotrophs and heterotrophic prokaryotes (Fig. 3B,

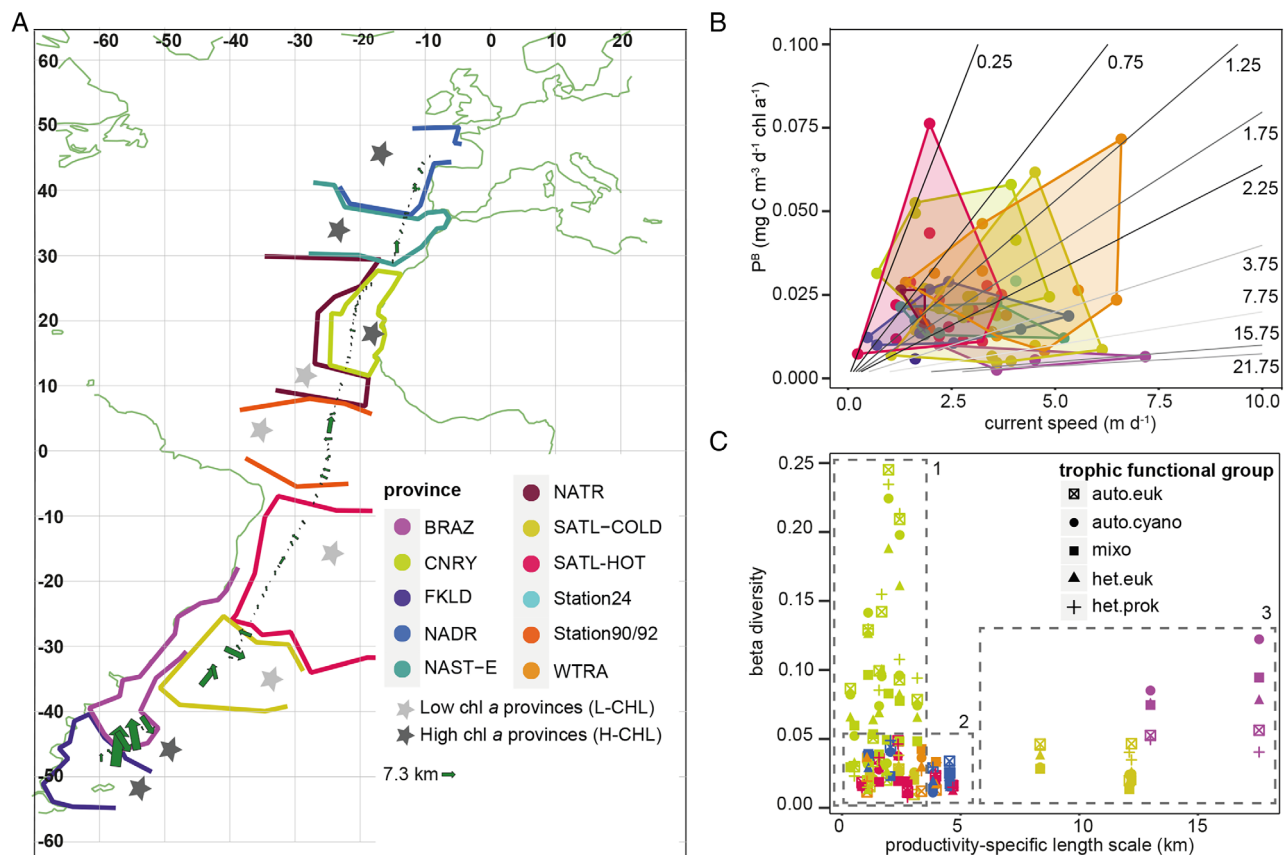


**Fig. 2.** (A) Map of the PS113 expedition indicating productivity specific length scale using a quantitative comparison of measured biomass turnover [half of standing stock phytoplankton biomass (chl *a* concentration) is replaced by new biomass (calculated from primary productivity rates) and measured horizontal current speed (ADCP horizontal velocity)], see Eqs. 3 and 4 for more details. Direction is derived from ADCP measurements. Ocean provinces are indicated with coloured lines. Light grey stars indicate low-chl *a* provinces, dark grey stars indicate high-chl *a* provinces.

B. Specific primary productivity ( $P^B$ ) against current speed ( $\text{m d}^{-1}$ ) at each site. Sites are colour coded according to ocean provinces. Productivity-specific length scales (km) are indicated by grey lines across the plot.

C. Beta diversity to neighbouring sites based on ordination distances against productivity-specific length scales for each trophic functional group. Sites are colour coded according to ocean provinces. Box 1 indicates high beta diversity with great variability within the CNRY province. Box 2 corresponds to beta diversity variation of most ocean provinces with an upper limit of 5 km productivity-specific length scale; box 3 indicates an increase in beta diversity with productivity-specific length scales > 5 km.

Table S3). POC, PN and chl *a* were significantly negatively correlated with the  $\alpha$ -diversity of autotrophic eukaryotes. The  $\alpha$ -diversity of heterotrophic prokaryotes was negatively correlated with  $\text{NO}_3$ ,  $\text{PO}_4$ , POC, PN (Fig. 3B; Table S3). However, *within* provinces, we found both positive and negative correlations of functional groups with temperature, nutrients and particulate matter (e.g. PN correlated positively with cyanobacterial diversity in the SATL-COLD province:  $r = 0.8$ ,  $p = 3.85 \times 10^{-4}$ ,  $n = 15$ , Fig. 3B).

PP had no significant correlations with picoplankton cell number or microbial  $\alpha$ -diversity across any trophic functional group (Table S3). However, in the CNRY province, where productivity rates were significantly higher than in other provinces (Wilcoxon,  $p$ -value =  $5.75 \times 10^{-4}$ ,  $n_1 = 17$ ,  $n_2 = 77$ ), diversity of autotrophic eukaryotes and

cyanobacteria were negatively correlated with PP ( $r = -0.6$ ,  $p = 0.04$ ,  $n = 14$ , and  $r = -0.6$ ,  $p = 0.01$ ,  $n = 14$  respectively; Fig. 3B).

We noted that  $\alpha$ -diversity of trophic functional groups are similarly structured in their correlations with environmental (physical + chemical) parameters; however, the magnitudes and significances of the correlations varied between groups (e.g. NAST-E  $\text{PO}_4$ , auto.cyano;  $r = 0.83$ ,  $p = 0.01$ ;  $\text{PO}_4$ , het.prok,  $r = 0.39$ ,  $p = 0.27$ , Figs S6 and S7), as did the distribution of residuals (Figs S8–S15). Between functional groups, we observed a significant positive correlation between the  $\alpha$ -diversity of autotrophic eukaryotes and cyanobacteria in the CNRY provinces or between autotrophic eukaryotes and mixotrophs in the CNRY and NADR provinces as well as across the transect (Fig. 3B, S16).



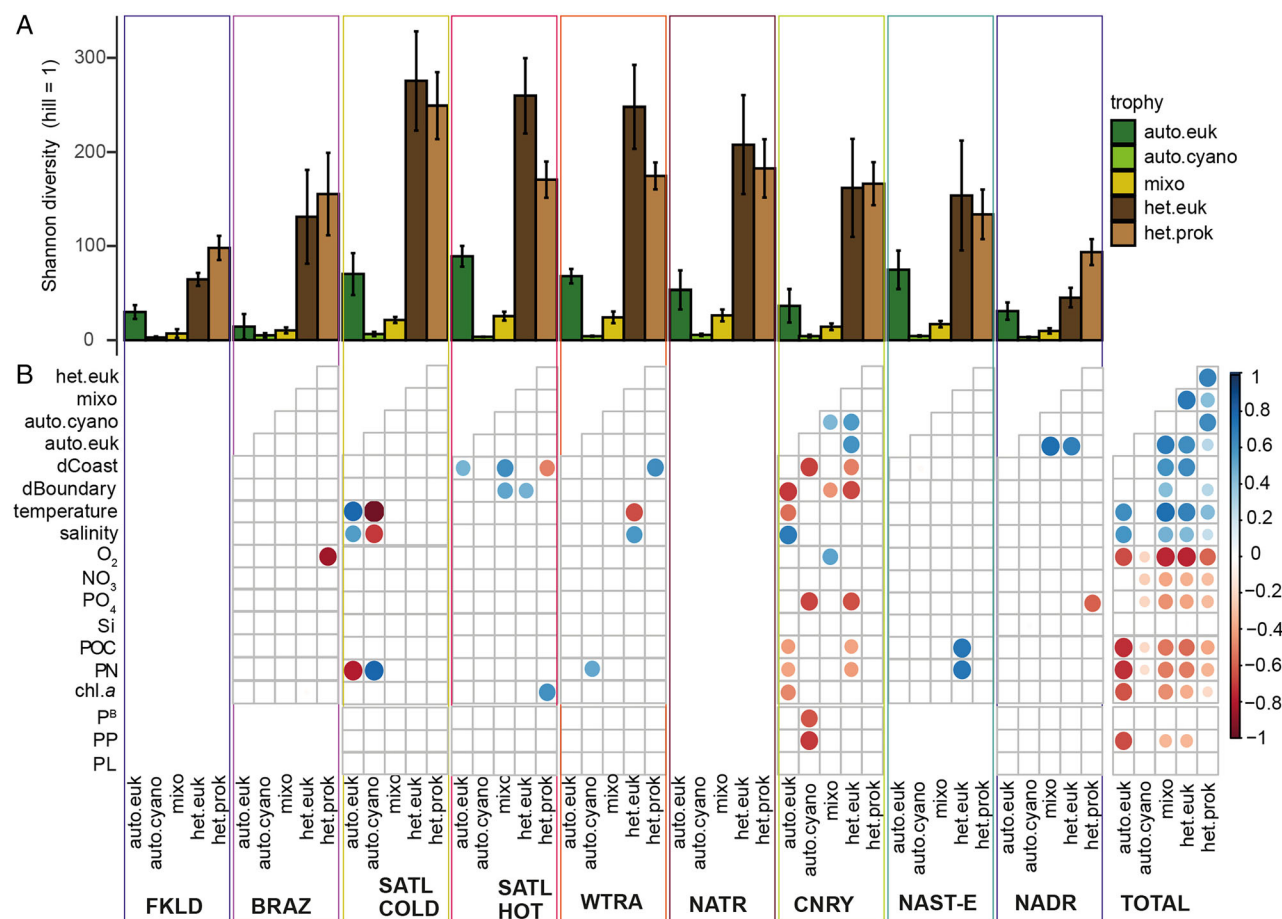


**Fig. 3.** Alpha diversity across ocean provinces.

A. Mean microbial Shannon diversity of eukaryotic autotrophs, prokaryotic autotrophs (cyanobacteria), eukaryotic mixotrophs, heterotrophic eukaryotes and heterotrophic prokaryotes; Error bars indicate standard deviation of microbial Shannon diversity within each province. Sample size within each province is indicated below.

B. Pearson correlations of Shannon diversities with and environmental parameters within ocean provinces. Distance to coast (dCoast) calculated as distance of sample to next shore (in kilometer), dBoundary is the distance to the province boundary of the sample identified to belong to, temperature is sea surface temperature ( $^{\circ}\text{C}$ ), salinity is sea surface salinity, oxygen ( $\mu\text{M}$ ), nitrate ( $\text{NO}_3$ ) in  $\mu\text{M}$ , phosphate ( $\text{PO}_4$ ) in  $\mu\text{M}$  Silicate (Si) in  $\mu\text{M}$ , Particulate organic carbon concentration (POC) in  $\text{nM}$ , particulate nitrogen (PN) concentration in  $\text{nM}$ , chlorophyll *a* (chl *a*) in  $\text{mg m}^{-3}$ , specific primary productivity ( $P^B$ ) in  $\text{nmol C L}^{-1} \text{ h}^{-1}$  chl *a* $^{-1}$ , primary productivity (PP) in  $\text{nmol L}^{-1} \text{ h}^{-1}$ . Correlation plots with colours indicating gradient from negative (red) to positive (blue) correlation; correlations of not significant, i.e.  $p$ -value  $> 0.05$ , and with non-normal distribution of residuals in linear regression model were removed from the plot [for full correlation plot see Fig. S6, and Figs S8–S14 for residual histogram plots of individual provinces and across the entire transect (Fig. S15)]. Within provinces, correlations were calculated for eukaryotes and prokaryotes respectively, and each trophic group (autotroph, mixotroph and heterotroph) against different environmental variables and against each other. Coloured boxes indicate correlations within provinces: FKLD, Southwest Atlantic Shelves province ( $n = 4$ ); BRAZ, Brazil Current Coastal province ( $n = 8$ ); SATL, South Atlantic Subtropical Gyral province (COLD:  $n = 15$ ; HOT:  $n = 20$ ); WTRA, Western Tropical Atlantic province ( $n = 17$ ); NATR, North Atlantic Tropical Gyral province ( $n = 6$ ); CNRY, Canary Current Coastal province ( $n = 26$ ); NAST, North Atlantic Subtropical Gyral province ( $n = 10$ ); NADR, North Atlantic Drift province ( $n = 13$ ). ALL indicates all samples across the entire transect ( $n = 121$ ).

We observed that each province has a distinct correlation pattern across the variables we examined (Fig. 3B). Correlations were more pronounced in the CNRY province (Fig. 3B). We could not identify pairs of parameters with correlations that were consistently repeated across provinces (e.g. temperature, auto.euk SATL-COLD; temperature, auto.euk SATL-HOT; Fig. 3B). Furthermore, we noted that samples were not evenly spread along bivariate plots, especially in

physically energetic regions (i.e. large scatter of temperature – salinity profile; Fig. S17).

#### *Beta diversity ( $\beta$ -diversity) patterns of auto-, mixo- and heterotrophs across provinces*

Sites belonging to high-chl *a* and low-chl *a* provinces were well separated along the first axes of our redundancy analysis (RDA) plots for each trophic functional

group (Fig. 4; between 40% and 61% of variance constrained). Sites belonging to high-chl *a* provinces were associated with higher dissolved inorganic nutrient concentrations, particulate organic matter and chl *a* concentrations. Sites belonging to low-chl *a* provinces were associated with higher temperatures, salinity and larger distances to province boundaries and the coast.

We found that sites in low-chl *a* and high-chl *a* provinces were differentially ordinated in our RDA biplots. We observed the shortest distances between sites in low-chl *a* provinces when analysing autotrophic eukaryotic diversity. In contrast, heterotrophic eukaryotic and mixotrophic diversity led to sites in low-chl *a* provinces being ordinated furthest apart from those in other provinces (Table S4). While autotrophic eukaryotic communities were distinctly separated between the high-chl *a* provinces, mixotrophic communities had short relative ordination distances or overlapped in these provinces (Fig. 4A and C; Table S4). Across all trophic groups, the samples from the CNRY province showed the largest spread among the second RDA axes and partially overlapped with samples from the NAST-E province (Fig. 4).

Prokaryotic heterotrophic communities were more similar to autotrophic eukaryotes in their pattern of the biplots (procrustes analysis, Table S5), with shorter relative distances in low-chl *a* than in high-chl *a* provinces (Fig. 4A and E; Table S4). In contrast, cyanobacteria, heterotrophic and mixotrophic eukaryotes were more similar to each other (procrustes analysis, Table S5); shorter relative distances in high-chl *a* than in low-chl *a* provinces (Fig. 4; Table S4).

Analysis of the  $\beta$ -diversity among communities of heterotrophic pro- and eukaryotes, and mixotrophs ordinated station 24 between those that are characteristic of the BRAZ province and the southern, cold part of the SATL-COLD province (Fig. 4C–E). Similarly, analysis of  $\beta$ -diversity of the autotrophic eukaryotes and mixotrophs at Station 92 (located between the SATL-HOT and the WTRA province) ordinated the station between the SATL-HOT and WTRA (Fig. 4A and C).

The SATL province, as defined by Longhurst (2007), clustered into two distinct groups in microbial  $\beta$ -diversity (Fig. 4) which was also apparent in our biogeochemical inspection and division into a southern dynamic (COLD) part, and a northern, oligotrophic (HOT) part in the Brazil Basin (Fig. 4).

## Discussion

Our study revealed that microbial trophic groups showed variable  $\alpha$ - and  $\beta$ -diversity patterns in relation to physical and biogeochemical environmental parameters across our south-to-north transect. Below, we discuss how our integrative results can contribute to refining microbial,

biogeographic provincialism. Our results provide an estimate of sample-based spatial scales of differences in biodiversity signals, suggesting that observations of ecosystem function and stability need regional high-resolution sampling.

*In situ measurements of province characteristics deviate from Longhurst provinces.* Broadly, traditional Longhurst province boundaries (Longhurst, 2007) are determined by clustering remote sensing data on chl *a* and temperature data (e.g. Devred *et al.*, 2007; Hardman-Mountford *et al.*, 2008) or *in situ* measurements of phytoplankton pigment composition (Barlow *et al.*, 2007; Taylor *et al.*, 2011; Bracher *et al.*, 2020). Our delineation largely overlapped (for about 80% of the stations) with the provinces delineated by Bracher *et al.*, (2020) using hierarchical cluster analysis on phytoplankton group composition data derived from the HPLC marker pigments (Table S6). However, we observed regional divergence. Most pronounced was the separation of the SATL province into SATL-HOT and SATL-COLD; supported by our physical, chemical and microbial observations. This difference could not be detected in phytoplankton pigment-based analyses (see Bracher *et al.*, 2020). Such observations (if confirmed) exemplify how new provincialisation can arise from microbial oceanographic perspectives.

However, we also noted that some of our *in situ* measurements could lead to spurious distinctions within provinces. For example, we occasionally measured high nutrient and chl *a* concentrations in provinces known to be oligotrophic (Longhurst, 2007; e.g. up to  $0.43 \text{ mg m}^{-3}$  chl *a* in the NATR province). Given our sampling regime, this may simply be the result of sampling a transient patch of high-nutrient/high-chl *a* water. Our  $\beta$ -diversity supports this possibility, as NATR sites were largely ordinated with sites from other oligotrophic provinces along the first major axis in each of our RDA triplots (Fig. 4). We note that this shows the value of microbial diversity data in holistically describing oceanographic provinces, especially when sampling dynamic regions.

Ocean currents can drive overlaps in  $\beta$ -diversity signals: For example, ordinations showed that sites from the NAST-E and CNRY province overlapped (Fig. 4), likely caused by transport and dispersal along the Azores Current which joins the Canary Current (Fedoseev, 1970; Fig. S2a). The complex dynamics in the CNRY province (driven, for example, by a weakening of the Canary Current through coastal upwelling and eddy formations as described in accompanying studies of the same sampling campaign; (Bracher *et al.*, 2020; von Appen *et al.*, 2020) likely contributed to increased microbial  $\beta$ -diversity, relative to most other provinces. Similarly, samples in physically energetic provinces (e.g. BRAZ province), defined by an increased scatter in their temperature-salinity

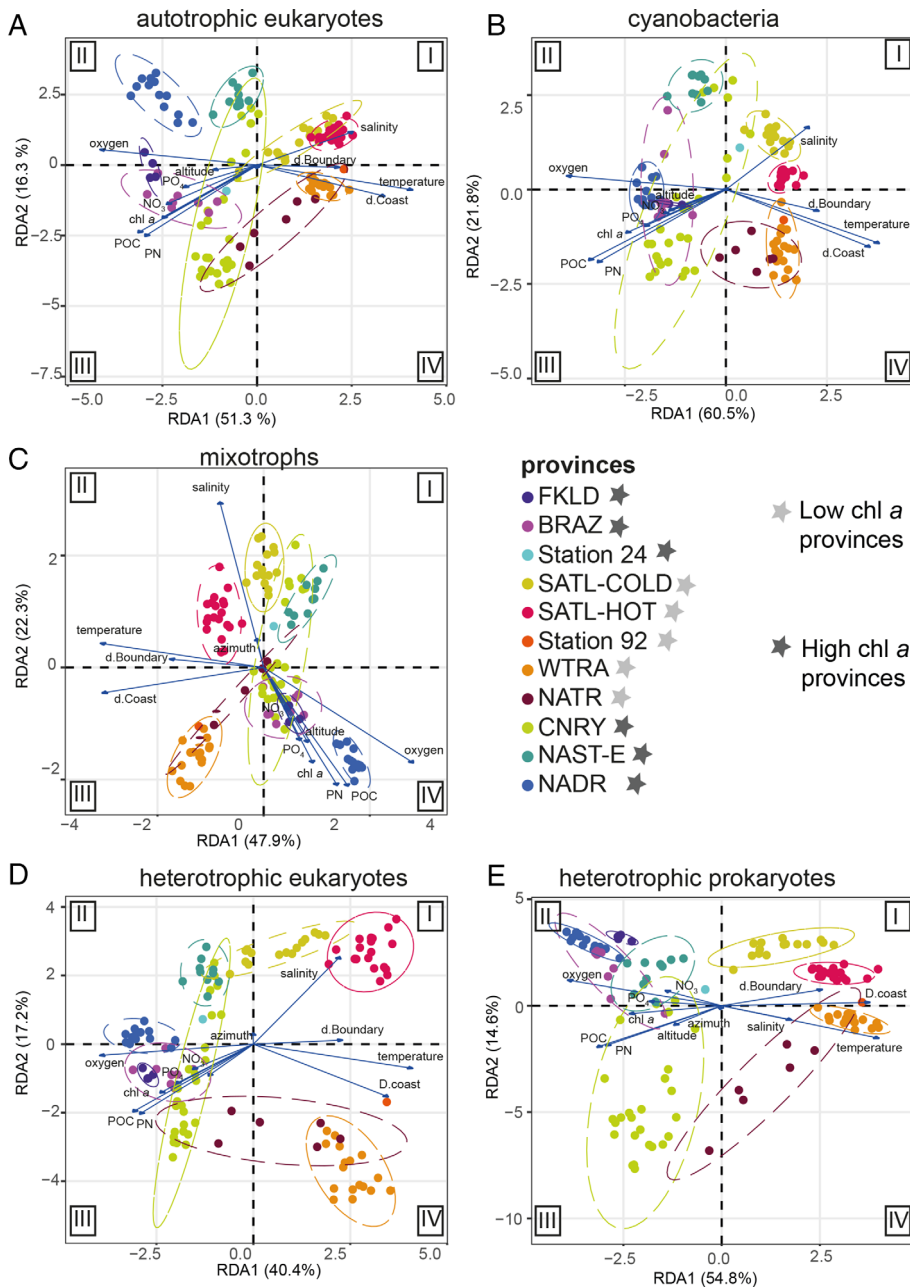


**Fig. 4.** Redundancy analysis (RDA) of CLR-transformed ASV counts, subsequently partitioned into separate tables for each functional group (A) autotrophic eukaryotes, (B) autotrophic prokaryotes (C) eukaryotic mixotrophs, (D) heterotrophic eukaryotes and (E) heterotrophic prokaryotes. Contextual spatial and environmental data (z-scored) were used as explanatory variables, represented as arrows. Samples cluster according to ocean provinces. Samples separate between low-chl *a* provinces (SATL-COLD, SATL-HOT, WTRA, NATR) (indicated with light grey star) and high-chl *a* provinces (FKLD, BRAZ, CNRY, NAST-E, NADR) (indicated with dark grey star) along the first axis (RDA 1) across all functional groups.

profiles (Figs S2 and S17), were more distributed in their  $\alpha$ -diversity suggesting that the habitat structure is more disrupted or patchy in these ecosystems and high-resolution sampling (<50 km) is needed for stable biodiversity assessments as shown in other studies across ocean filaments (Fadeev *et al.*, 2021) and fronts (Mousing *et al.*, 2016).

**Productivity-specific length scales and their role in microbial biogeography.** The ratio of PP rate and current speed gives us a productivity-specific length over which a biological community is carried during a single biomass

turnover. This can be interpreted as a scale relating the potential for observed changes in  $\beta$ -diversity to horizontal transport. This may be seen as a time-sensitive version of earlier relationships described between chl *a* patchiness and current speed (Powell *et al.*, 1975). Specifically, we estimated the PP rate (normalized  $P^B$ ) at each sampling site through  $^{13}\text{C}$  stable isotope experiments and biomass assessment (chl *a* concentration). The advective environment in which this growth occurs was characterized through measuring surface current speed – in  $\text{m d}^{-1}$  – at each sampling point. Overall, the productivity-specific length scale provides a first-order



estimate of the spatial scale of ecosystem patchiness in epipelagic systems, ultimately controlled by a key biological rate (PP) and horizontal current speed.

Across the Atlantic, we identified three regimes of  $\beta$ -diversity associated with different magnitudes of productivity-specific length scales [high diversity at low productivity-specific length scales (Fig. 2C Box 1), low diversity at low productivity-specific length scales (Fig. 2C Box 2), and increasing diversity with increasing productivity-specific length scales (Fig. 2C Box 3)], affected by different magnitudes of  $P^B$  and current speed within different provinces (Fig. 2B).

For example, prokaryotic growth in oligotrophic regions with low current speed, such as the SATL-HOT province, has been shown to be controlled by heterotrophic grazing (Teira *et al.*, 2019). In our data, the change in  $\beta$ -diversity within the SATL-HOT province occurred at intermediate productivity-specific length scales with higher  $P^B$ , higher proportional heterotrophic biomass and higher eukaryotic heterotrophic richness relative to other sites (Fig. 2B and C – box 2, Tables S1 and S2). This can suggest that differences in productivity-specific length scales are a result of greater biological top-down control on local biodiversity than differences in horizontal current speed. The  $\beta$ -diversity signals in provinces with high horizontal current speed increased with increasing productivity-specific length scales (Fig. 2C box 3 SATL\_COLD, BRAZ), suggesting a possible shift in mechanisms for  $\beta$ -diversity at higher productivity-specific length scales. The observed increase in  $\beta$ -diversity was likely due to the variable local energetics of the Brazilian Coastal Current (De Souza and Robinson, 2004); reflected in a large range of temperature-salinity signals in our dataset (Fig. S2). These energetics can result in a confluence zone of communities potentially far from their region of origin (Malvinas-Brazil Confluence; Clayton *et al.*, 2013). However, at this point, we cannot differentiate between the physical and biological mechanisms as we also observed different magnitudes of ordination distances within different trophic functional groups. For most of our sites (Fig. 2C, Box 2), the length scale was <5 km and did not correlate with the relatively low  $\beta$ -diversity signals in our RDA analyses (<0.05 ordination distance). In this case,  $\beta$ -diversity can be controlled by one or more of the multiple environmental variables shaping microbial communities such as vertical mixing (Cheng *et al.*, 2020), atmospheric processes (Mayol *et al.*, 2014), macroorganisms (Troussellier *et al.*, 2017) and anthropogenic impact (Nogales *et al.*, 2011).

It is important to note that at this point, we discuss surface dynamics only, and do not include any consideration of vertical mixing, itself clearly an important feature in generating diversity changes (Delong *et al.*, 2006), and likely the source for the great heterogeneity of  $\beta$ -diversity

in the CNRY province (Fig. 2C – Box 1). Understanding the interplay of biological and physical controls would require more complete analyses of biological and physical interactions and is thus only a first-order estimate.

Essentially, the productivity-specific length scale can be seen as defining a relevant scale of the mosaic of the biodiversity signatures measured in this study, revealing where higher-resolution sampling (<5 km) would have added more value to our data set and thus where more careful interpretations of our  $\beta$ -diversity results are necessary. It also provides a perspective on the resolution future campaigns should adopt to develop biogeographic understandings in each region.

We are convinced that Lagrangian sampling – at scales informed by sample-based productivity-specific length scales – could enhance our understanding of microbial pelagic biogeography. This approach would help characterize how far microbial communities in a given water packet could disperse within provinces boundaries, giving shape to their internal mosaics of biodiversity. This is analogous to how the Damköhler number relates exposure timescale and processing timescale of a chemical reaction, to express how spatially and temporally extended the impacts of that reaction will be felt (Oldham *et al.*, 2013).

*Province-dependent correlation structures between  $\alpha$ -diversity and environmental variables.* Across our entire transect, correlations between microbial  $\alpha$ -diversity and environmental variables followed well-described latitudinal temperature–diversity relationships (e.g. Fuhrman *et al.*, 2008; Ibarbalz *et al.*, 2019). However, we observed more faceted environment–diversity relationships within provinces, especially within physically energetic provinces (Fig. 3B). More measured variables, including temperature, correlated with  $\alpha$ -diversity in energetic provinces relative to those with less energetic profiles. This suggests that the temperature–diversity relationship is not controlled by thermal energy alone (see, e.g. Giebel *et al.*, 2009) but is nested in a more faceted microbial response to local water mass characteristics. For example, the high-temperature provinces we sampled were also oligotrophic (low chl *a*), which would confound any attempt to independently assess temperature–diversity relationships without accounting for the impact of oligotrophic conditions on  $\alpha$ -diversity (Fig. 3A; Santi *et al.*, 2019).

Our results showed a nuanced relationship of PP to microbial  $\alpha$ -diversity within provinces and do not corroborate previous observations, which detected significant positive correlations (Raes *et al.*, 2018). We observed moderate positive (but not significant at  $n = 20$ ) correlations of PP and prokaryotic heterotrophic  $\alpha$ -diversity in low-chl *a* provinces. This may be due to more

oligotrophic conditions supporting more even saturation of available niches, rather than boom-and-bust dynamics characteristic of eutrophic environments and events (Duffy and Stachowicz, 2006). In contrast, we observed a negative and significant correlation between  $\alpha$ -diversity and PP in the highly productive CNRY province, suggesting the rise and succession (via invasibility) of a few, opportunistic phylotypes (Steiner and Leibold, 2004), due to input of limiting nutrients from Saharan dust (von Appen *et al.*, 2020). Together, our observations in the Atlantic and those in the Pacific (Raes *et al.*, 2018) suggest that the relationship between PP and microbial  $\alpha$ -diversity is nuanced, and observed signals depend on province-specific characteristics, which drive competition.

Notably, the differences in sampling size ( $n_{\min} = 8$ ,  $n_{\max} = 20$ ) of different provinces impact individual correlation and correlation significance. Thus, we excluded the FKLD ( $n = 4$ ) and NATR ( $n = 6$ ) province from our correlation analysis. The great variability in significant correlations between environmental variables and microbial diversity showed that refined observations within provinces are needed to confirm the observed individual environment–diversity relationships.

*Low and high chl a conditions correspond to contrasting diversity patterns between trophic groups.* We observed contrasting  $\beta$ -diversity patterns in microbial functional groups associated with low- and high-chl a conditions, supporting the observations by Irwin *et al.* (2006) of differences in the importance of environmental predictors for different phytoplankton functional types. Our results show that environmental conditions are important predictors not only on a phylogenetic level (e.g. diatoms vs. dinoflagellates, Irwin *et al.*, 2006) but also within trophic functional groups.

We observed that eukaryotic mixotrophic communities had relatively high  $\alpha$ -diversity at each site and high  $\beta$ -diversity between sites in low-chl a provinces (vs. high-chl a provinces), suggesting that mixotrophy is supported under low-nutrient, low chl a conditions (see, e.g. Hartmann *et al.*, 2012). Similarly, the  $\beta$ -diversity of cyanobacteria and eukaryotic heterotrophs was greater in sites under low chl a conditions, suggesting these functional groups are more susceptible to selective forces in these provinces (e.g. increased cyanobacterial diversity under low phosphate conditions; Thompson *et al.*, 2013).

In contrast, we observed that there is greater  $\beta$ -diversity between sites across high-chl a provinces (vs. low-chl a provinces) when examining eukaryotic autotrophic and prokaryotic heterotrophic communities (Fig. 4A and E), which are known to structure one another (Seymour *et al.*, 2017). However, we did not observe any proportional change in the  $\alpha$ -diversity of these groups between low- and high-chl a provinces.

This suggests that higher productivity is contributing more to species turnover between sites, rather than greater diversity within sites (Vallina *et al.*, 2014). Observing a stable number of Hutchinsonian niches suggests that their occupancy is driven more by stochastic than deterministic processes in these provinces. These processes may include the dilution of slow-growing cells in dynamic systems (Irwin *et al.*, 2006) as well as the prevalence and favouring of r-strategists in the community. However, further work is needed to explore these speculations.

Overall, our results extend previous findings (Legendre, 1981) of coupling between microbial diversity and productivity, showing trophic-specific diversity patterns between low chl a and high chl a conditions. Only more temporally and spatially expanded observations (factoring in functional diversity using metagenomics/transcriptomics, improved hydrographic descriptions, and physicochemical/nutrient profiles in these regions would allow our observations to be more confidently linked to ecosystem states driven by productivity (Chase and Leibold, 2002) and broader biogeographic descriptions.

## Conclusion

Here, we assessed how measures of microbial diversity and activity can better inform ecological partitioning of the ocean, granting new perspectives on functional microbial biogeography across, within and between provinces. We showed that eukaryotic autotrophs and prokaryotic heterotrophs show similar cross-province  $\beta$ -diversity patterns, distinct from those shared by mixotrophs, cyanobacteria and eukaryotic heterotrophs. Our calculations of a productivity-specific length scale are, to our knowledge, the first attempt to quantify – on a per-sample basis – the influence of surface ocean currents on microbial communities coupled to PP measurements. This provides a first-order estimate of how spatially extended a microbial diversity signature may be, and thus the scale of a recognizable patch in a larger biogeographic area. Our findings also show the value of exploring functional communities (i.e. guilds) of microorganisms to more holistically understand community ecology with phylogenetic diversity data. We conclude that highly resolved sampling of these factors along more Lagrangian designs would help microbial ecology coherently map the subdivisions of the ocean's biogeographic provinces.

## Materials and methods

### Sample collection

Our sampling was part of the PS113 (ANT-XXXIII/4) campaign onboard *RV Polarstern* from Punta Arenas, Chile,

to Bremerhaven, Germany, from 2018-05-08 to 2018-06-10 (Strass, 2018). We took discrete measurements for biophysical analyses of sea surface water at 193 stations in the Atlantic Ocean from about 11 m depth through the ship's seawater system (Teflon® tubing with a membrane pump) at an interval of ~0.5° latitude.

#### Province delineation after Longhurst

We defined ecological regions based on the variables suggested by Longhurst (2007), which include gradients in sea surface temperature, salinity, chl *a*, and checked for

$$PP = \frac{\text{at.\%}(\text{enriched}) - \text{at.\%}(\text{NA}) \times \text{POC}}{(100 \times (\text{DIC}(13\text{C}) \div (\text{DIC}(13) + \text{DIC}(12\text{C}))) - \text{at.\%}(\text{NA}) \times \text{Incubation time}} \quad (1)$$

matches in nutrient concentrations (Supplementary S1, Figs S1 and S2). We classified samples into provinces by identifying (i) clusters on a temperature-salinity plot (i.e. by water mass) where clusters were constrained by geographic proximity (Fig. S2), and (ii) boundary currents that coincided with province boundaries (i.e. where surface velocity vectors (geostrophic currents) were strong at province boundaries as identified above; Fig. S3a; Copernicus, 2020). We also identified ocean ridges in bathymetry profiles as features potentially structuring the modified provinces (GEBCO 2019). We compared our classification into Longhurst provinces with delineations proposed by Bracher *et al.* (2020) (Table S6).

We classified provinces as high-chl *a* provinces if their mean chl *a* concentrations were above 0.3 µg m<sup>-3</sup> chl *a*, or as low-chl *a* provinces if their mean concentrations were below 0.1 µg m<sup>-3</sup> chl *a*. Provinces with mean concentrations between 0.1 and 0.3 µg m<sup>-3</sup> were treated as ambiguous, and we defaulted to classifications in Longhurst (2007). For details see Supplementary S1.

We calculated the distances to the coast and to province boundaries in qgis 3.14 (QGIS Geographic Information System, 2020) by densifying the vector coastlines and extracting vertices, followed by extracting the distance from each site points to the nearest hub on the coast contours. We used the '110 m vector coastline' (v4.1.0, Natural Earth Data) and the province boundaries (delineated above) in our calculations.

#### Biochemical and PP profiling

At each station, we collected biochemical samples for dissolved inorganic nutrients (silicate, phosphate, nitrate

and nitrite) as well as particulate organic matter (POC and PN). For details see Supplementary S2.

We measured PP with 200 µmol NaH<sup>13</sup>CO<sub>3</sub> stable isotope incubations in triplicates over a time period of ~24 h. For details on experimental design see Supplementary S3 and incubation conditions in Table S7. Analysis of <sup>13</sup>C incorporated into organic matter was carried out on a PDZ Europa ANCA-GSL elemental analyser interfaced to a PDZ Europa 20-20 isotope ratio mass spectrometer (Sercon, Cheshire, UK) by the Isotopic Laboratory at the UC Davis, California campus. PP was calculated as in Eq. 1:

with at.\%(enriched) as the atom percent derived from <sup>13</sup>C-spiked samples; at.\%(NA) is the atom percent of natural abundance derived from particulate organic carbon (POC) samples. Dissolved inorganic carbon (DIC) is assumed as 2000 µmol kg<sup>-1</sup> (after Zeebe and Wolf-Gladrow, 2001). Incubation time is the time between sample spike and filtration (~24 h).

We calculated specific PP (*P<sup>B</sup>*) based on PP and chl *a* concentration, as shown in Equation 2.

$$P^B = \frac{PP}{\text{chl } a} \quad (2)$$

where PP is expressed in mg C m<sup>-3</sup> d<sup>-1</sup> and chl *a* concentration in mg chl *a* in m<sup>-3</sup>, resulting in a *P<sup>B</sup>* value in mg C m<sup>-3</sup> d<sup>-1</sup> chl *a*<sup>-1</sup>.

#### Productivity-specific length scale

To link the biomass turnover of microbial communities to their pelagic advection, we calculate a length scale for biological-physical coupling (productivity-specific length scale) using a quantitative comparison of measured biomass turnover and measured current speed.

$$\text{productivity} - \text{specific length scale} = \ln(2) \times \text{current speed} \times \lambda^{-1} \quad (3)$$

where the productivity-specific length scale is expressed in kilometer. Current speed reflects average horizontal current speed from the VM-ADCP which provided data

for the depth range 20–50 m. The  $\lambda$  is derived as in Eq. 4.

$$\lambda = \frac{\text{PP}}{\text{standing stock biomass}} \quad (4)$$

PP is expressed in  $\text{mg C m}^{-3} \text{ d}^{-1}$  and the standing stock biomass corresponds to the chl *a* concentration (in  $\text{mg m}^{-3}$ ) times 23  $\text{mg chl a (mg C)}^{-1}$  [for conversion between chl *a* and carbon concentrations (Geider, 1987); validated against *in situ* POC concentrations; Table S8].

#### Microbial sampling, processing and amplicon sequence analyses

**Flow cytometry.** At each station, samples for cell counts were taken into 2 ml Eppendorf tubes and incubated in the dark prior to fixation using 0.2% paraformaldehyde. Samples were snap-frozen and stored at  $-80^{\circ}\text{C}$  while at sea. Samples were analysed on a BD Accuri™ C6 Plus Flow Cytometer (BD Biosciences-US) according to Gasol and Moran (2015). For details on measurements see Supplementary S4.

**Microbial DNA sampling.** For 16S and 18S rRNA gene sequencing analysis, 4 L of seawater were filtered through 0.2  $\mu\text{m}$  Sterivex® filters. Filters were purged with air, tightly closed, snap-frozen in liquid nitrogen, and stored at  $-80^{\circ}\text{C}$  until further analysis.

**DNA extraction and amplicon sequencing.** DNA was extracted using a DNeasy® PowerWater® DNA extraction kit (QIAGEN, Valencia, CA, USA, Catalogue No./ID: 14900) following the manufacturer's instructions. After DNA extraction, DNA concentration was quantified using a Quantus™ Fluorometer and normalized to 2  $\text{ng } \mu\text{L}^{-1}$ .

Amplicons targeting the variable region 4 (V4) of the bacterial 16S rRNA gene (515F - 806R) (Caporaso *et al.*, 2016) and the variable region 4 (V4) of the eukaryotic 18S rRNA gene (TA-Reuk454FWD1 - TAR-eukREV3) (Stoeck *et al.*, 2010) were generated following standard protocols of amplicon library preparation (16S Metagenomic Sequencing Library Preparation, Illumina, Part #15044223 Rev.B) and sequenced using a MiSeq Sequencer (Illumina). 16S and 18S rRNA gene amplicon reads were generated using 300-bp paired-end sequencing using Nextera XT Index Kit v2 Set A-B (Illumina) index primer. Samples were demultiplexed using bcl2fastq (Illumina) with barcode mismatches set to 1.

ASV tables for both 16S and 18S rRNA gene amplicon sequences were constructed using the DADA2 R package, v1.15.1 (Callahan *et al.*, 2016). Samples were processed using the DADA2 pipeline (v.1.15) with an additional step where primers were trimmed using

cutadapt v1.18 after pre-filtering of FASTQ files (dada2\_16S.R, dada2\_18S.R in Supplementary\_Code/dada2/). Diagnostics of each filtering step are in Table S9 and number of reads plotted for each filtering step in density plots (Fig. S18).

**Taxonomic assignment and functional grouping.** Taxonomic assignment was performed outside DADA2 using SilvaNGS (v1.4) (Quast *et al.*, 2013) pipeline for 16S rRNA gene data with the similarity threshold set to 1. Reads were aligned using SINA v1.2.10 (Pruesse *et al.*, 2012), and classified using BLASTn (v2.2.30) (Camacho *et al.*, 2009) with the Silva database (v132) as a reference database (Supplementary 2). For taxonomic assignment of 18S rRNA gene amplicons, we used the QIIME 2 Plugin 'feature-classifier' (v2019.7.0 from package 'q2-feature-classifier') in qiime 2 (Bokulich *et al.*, 2018) and the pr2 database (v4.12) (Guillou *et al.*, 2013).

We classified eukaryotic taxa as either autotroph, mixotroph, heterotroph, or unknown if no information of trophic was available by performing an unstructured literature search to validate expert-led assignment by UJ (see outcomes in Table S10). Prokaryotes, except Cyanobacteria, were considered to be dominated by a heterotrophic lifestyle (*sensu* Herndl *et al.*, 2008), see Table S10 for further details.

#### Ecological data analyses

We performed our data analysis using R v4.0.3 (R Core Team, 2020) and RStudio v1.4.1103 (RStudio Team, 2021). Biophysical parameters, concentrations of particulate organic matter, dissolved inorganic nutrients, microbial cell counts and PP measurements were used as environmental metadata for statistical analyses with microbial sequencing data.

Alpha diversity ( $\alpha$ -diversity) was determined by calculating Hill numbers (Chao *et al.*, 2014) of richness, Shannon entropy and Simpson concentration ( $q = 0$ ,  $q = 1$  and  $q = 2$ ), using the iNEXT package (v2.0.20) repeating calculations 100 times (Supplementary\_Code/alpha\_diversity/alpha\_diversity.R). Rarefaction curves of all Hill numbers were plotted using fortify() of the ggplot2 package (v3.3.3). Further analyses were performed using Shannon diversity measures of each trophic functional group, as it reflects true diversity (richness + evenness) and is less susceptible to fluctuations in rarer phylotypes.

Pearson correlations between microbial Shannon diversity and environmental parameters (salinity, temperature,  $\text{PO}_4^{3-}$ ,  $\text{H}_4\text{SiO}_4$ ,  $\text{NO}_3$ , dissolved oxygen, distance to province boundary, distance to coast, PN, POC, chl *a*) were calculated and plotted using the corplot() function of the corplot package (v0.84) and adjusted for multiple testing

using the Holm–Bonferroni method (Supplementary\_Code/correlation\_analyses/general\_corplot.R). Residuals of all correlations were screened for notable departures from Gaussian distributions, in which case these correlations were excluded from our results (Supplementary\_Code/correlation\_analyses/Residuals\_corplot.R; Figs S8–S15).

ASV tables and environmental metadata were transformed for comparability and statistical downstream analyses (general\_clr\_hellinger\_transformations.R, z-scoring\_subset.R in Supplementary\_Code/data\_transformations/). Before transformations, we removed all ASVs with  $\leq 3$  instances across all samples. Furthermore, before CLR transformation, we performed Bayesian-multiplicative treatments of zeros in the ASV tables using `cmultRepl()` function of the `zComposition` package (v1.3.4): this uses sample-wise totals to convert zero counts (which will lead to errors in log-ratios) into near-zero estimates, assuming undersampling rather than absence. To account for compositionality effects in our ASV tables (see Gloor *et al.*, 2017), we performed a CLR transformation for RDA. Prior to permutational MANOVA (PERMANOVA) analyses using the `decostand()` function in `vegan` (v2.5.6), Environmental variables were checked for normal distribution (Fig. S19) and z-scored for scale-independent intercomparability.

We examined the distribution of sites among environmental gradients using a PCA on our microbial diversity metadata. We tested differences of ocean provinces using two-sided Wilcoxon rank-sum tests (hereafter: Wilcoxon) (Supplementary\_Code/environmental\_analyses/PP\_plots.R L.81–84).

To examine microbial beta diversity ( $\beta$ -diversity) and its relation to environmental and contextual variables, we performed a set of RDA using the CLR-transformed ASV tables as response matrices and tables of environmental variables as explanatory matrices. We calculated sun azimuth and altitude based on sampling time and location using the `suncalc` (v.0.5.0) package in R. We performed stepwise model to identify significant environmental variables using `ordiR2step()` function in `vegan` (Supplementary\_Code/multivariate\_analysis\_ordistep.R). Differences of microbial dissimilarity between ocean provinces were tested with a PERMANOVA (Anderson, 2001) on Aitchinson distance of the CLR-transformed ASV tables using the `adonis2()` function along with a beta dispersion test to evaluate the homogeneity of dispersion using the `betadisper()` function in `vegan` (Supplementary\_Code/multivariate\_analysis/RDA\_functions.R).

## Acknowledgements

We thank Volker Strass and the crew of *RV Polarstern* for their support during the PS113 expedition. We thank Pauline Thome for her support in sampling during the expedition and Susanne Spahic for her help during the expedition. We thank

Simon Dreutter for help with the qGIS environment. We thank Dr. Wilken-Jon von Appen for his help in oceanographic data analyses. We thank Prof. Dr. Matthias Ullrich, Prof. Dr. Frank Oliver Glöckner as well as two anonymous reviewers for their comments on this study. This study was supported by the Helmholtz POLMAR Graduate School, the POF IV Research Programme topic 6 and subtopic 6.2 of the Alfred Wegener Institute, Helmholtz Centre for Polar and Marine Research, Germany. Research funding was further provided by the Ocean Frontier Institute, through an award from the Canada First Research Excellence Fund.

## Data Availability Statement

Chlorophyll *a* (chl *a*) data were derived from <https://doi.org/10.1594/PANGAEA.913514> and published in Bracher *et al.* (2020). Dissolved inorganic nutrients, particulate organic matter and primary productivity measurements are publicly archived (<https://doi.org/10.1594/PANGAEA.926458>, <https://doi.org/10.1594/PANGAEA.926460> and <https://doi.org/10.1594/PANGAEA.926462> respectively). Sequence data for this study have been deposited in the European Nucleotide Archive (ENA) at EMBL-EBI under accession number PRJEB42499 (<https://www.ebi.ac.uk/ena/browser/text-search?query=PRJEB42499>), using the data brokerage service of the German Federation for Biological Data [GFBio, (Diepenbroek and Glöckner, 2014)], in compliance with the Minimal Information about any (X) Sequence (MIxS) standard (Yilmaz *et al.*, 2011). The analysis based on satellite data was generated using E.U. Copernicus Marine Service Information and are available at <http://marine.copernicus.eu> (Copernicus, 2020) using the GLOBAL\_ANALYSISFORECAST\_PHY\_CPL\_001\_015 data (Lea *et al.*, 2015). The 110 m vector coastline (ESRI shapefile; v4.1.0) is available at <https://www.naturalearthdata.com/>.

## Code Availability

Statistical analysis code is available in the Supplementary\_Code supplement of this paper with documentation in an R Notebook (top-level directory) and all code files. Code is also publicly archived on github in the tagged release: <https://zenodo.org/badge/latestdoi/10.5281/zenodo.329689664> (released with publication).

## References

- Anderson, M.J. (2001) A new method for non-parametric multivariate analysis of variance. *Austral Ecol* **26**: 32–46.
- Azam, F., Fenchel, T., Field, J.G., Gray, J.S., Meyer-Reil, L. A., and Thingstad, F. (1983) The ecological role of water-column microbes in the sea. *Mar Ecol Prog Ser* **10**: 257–263.
- Azam, F., and Malfatti, F. (2007) Microbial structuring of marine ecosystems. *Nature* **5**: 782–791.



- Barlow, R., Stuart, V., Lutz, V., Sessions, H., Sathyendranath, S., Platt, T., *et al.* (2007) Seasonal pigment patterns of surface phytoplankton in the subtropical southern hemisphere. *Deep Res Part I Oceanogr Res Pap* **54**: 1687–1703.
- Bokulich, N.A., Kaehler, B.D., Rideout, J.R., Dillon, M., Bolyen, E., Knight, R., *et al.* (2018) Optimizing taxonomic classification of marker-gene amplicon sequences with QIIME 2's q2-feature-classifier plugin. *Microbiome* **6**: 1–17.
- Bracher, A., Xi, H., Dinter, T., Mangin, A., Strass, V., von Appen, W.J., and Wiegmann, S. (2020) High resolution water column phytoplankton composition across the Atlantic Ocean from ship-towed vertical undulating radiometry. *Front Mar Sci* **7**: 1–22.
- Cadotte, M.W. (2006) Dispersal and species diversity: a meta-analysis. *Am Nat* **167**: 913–924.
- Callahan, B.J., McMurdie, P.J., Rosen, M.J., Han, A.W., and Johnson, A.J.A. (2016) DADA2: high resolution sample inference from Illumina amplicon data. *Nat Methods* **13**: 581–583.
- Camacho, C., Coulouris, G., Avagyan, V., Ma, N., Papadopoulos, J., Bealer, K., and Madden, T.L. (2009) BLAST+: architecture and applications. *BMC Bioinformatics* **9**: 1–9.
- Caporaso, J.G., Laubner, C.L., Costello, E.K., Berg-Lyons, D., González, A., Stombaugh, J., *et al.* (2016) Moving pictures of the human microbiome. *Genome Biol* **36**: 50–80.
- Cardinale, B.J., Matulich, K.L., Hooper, D.U., Byrnes, J. E., Duffy, E., Gamfeldt, L., *et al.* (2011) The functional role of producer diversity in ecosystems. *Am J Bot* **98**: 572–592.
- Chao, A., Gotelli, N.J., Hsieh, T.C., Sander, E.L., Colwell, R. K., and Ellison, A.M. (2014) Rarefaction and extrapolation with hill numbers: a framework for sampling and estimation in species diversity studies. *Ecol Monogr* **84**: 45–67.
- Chase, J.M., and Leibold, M.A. (2002) Spatial scale dictates the productivity-biodiversity relationship. *Nature* **416**: 427–430.
- Cheng, W.H., Lu, H.P., Chen, C.C., Jan, S., and Hsieh, C.H. (2020) Vertical beta-diversity of bacterial communities depending on water stratification. *Front Microbiol* **11**: 1–10.
- Copernicus Marine Environment Monitoring Service (2020). Available at: <http://marine.copernicus.eu>.
- Clayton, S., Dutkiewicz, S., Jahn, O., and Follows, M.J. (2013) Dispersal, eddies, and the diversity of marine phytoplankton. *Limnol Oceanogr Fluids Environ* **3**: 182–197.
- De Souza, R.B., and Robinson, I.S. (2004) Lagrangian and satellite observations of the Brazilian coastal current. *Cont Shelf Res* **24**: 241–262.
- Delong, E.F., Preston, C.M., Mincer, T., Rich, V., Hallam, S. J., Frigaard, N., *et al.* (2006) Community genomics among stratified microbial assemblages in the ocean's interior. *Science* **311**: 496–504.
- Devred, E., Sathyendranath, S., and Platt, T. (2007) Delineation of ecological provinces using ocean colour radiometry. *Mar Ecol Prog Ser* **346**: 1–13.
- Diepenbroek, M., and Glöckner, F.O. (2014) Towards an integrated biodiversity and ecological research data management and archiving platform: The German Federation for the Curation of Biological Data (GFBio) INFORMATIK 2014 1711–1721.
- Duffy, J.E., and Stachowicz, J.J. (2006) Why biodiversity is important to oceanography: potential roles of genetic, species, and trophic diversity in pelagic ecosystem processes. *Mar Ecol Prog Ser* **311**: 179–189.
- Fadeev, E., Wietz, M., Von Appen, W.J., Iversen, M.H., Nöthing, E.-M., Engel, A., *et al.* (2021) Submesoscale dynamics directly shape bacterioplankton community structure in space and time. *Limnol Oceanogr*, **66**: 2901–2913. <https://doi.org/10.1002/lno.11799>
- Falkowski, P.G., Fenchel, T., and Delong, E.F. (2008) The microbial engines that drive earth's biogeochemical cycles. *Microb Ecol* **320**: 1034–1040.
- Fedoseev, A. (1970) Geostrophic circulation of surface waters on the shelf of north-West Africa. *Rapp PV Reun Cons Int Explor Mer* **159**: 32–37.
- Fuhrman, J.A., Cram, J.A., and Needham, D.M. (2015) Marine microbial community interpretation. *Nat Publ Gr* **13**: 133–146.
- Fuhrman, J.A., Steele, J.A., Hewson, I., Schwalbach, M.S., Brown, M.V., Green, J.L., and Brown, J.H. (2008) A latitudinal diversity gradient in planktonic marine bacteria. *Proc Natl Acad Sci U S A* **105**: 7774–7778.
- Gasol, J.M. and Moran, X. (2015) Flow cytometric determination of microbial abundances and its use to obtain indices of community structure and relative activity In: *Hydrocarbon and Lipid Microbiology Protocols. Springer Protocols Handbooks*, Springer, Berlin, Heidelberg.
- Geider, R.J. (1987) Light and temperature dependence of the carbon to chlorophyll a ratio in microalgae and cyanobacteria: implications for physiology and growth of phytoplankton. *New Phytol* **106**: 1–34.
- Giebel, H.A., Brinkhoff, T., Zwisler, W., Selje, N., and Simon, M. (2009) Distribution of Roseobacter RCA and SAR11 lineages and distinct bacterial communities from the subtropics to the Southern Ocean. *Environ Microbiol* **11**: 2164–2178.
- Gloor, G.B., Macklaim, J.M., Pawlowsky-Glahn, V., and Egozcue, J.J. (2017) Microbiome datasets are compositional: and this is not optional. *Front Microbiol* **8**: 1–6.
- Guidi, L., Chaffron, S., Bittner, L., Eveillard, D., Marin, M., and De Roscoff, S.B. (2016) Plankton networks driving carbon export in the oligotrophic ocean. *Nature* **532**: 465–470.
- Guillou, L., Bachar, D., Audic, S., Bass, D., Berney, C., Bittner, L., *et al.* (2013) The Protist ribosomal reference database (PR2): a catalog of unicellular eukaryote small sub-unit rRNA sequences with curated taxonomy. *Nucleic Acids Res* **41**: 597–604.
- Hardman-Mountford, N.J., Hirata, T., Richardson, K.A., and Aiken, J. (2008) An objective methodology for the classification of ecological pattern into biomes and provinces for the pelagic ocean. *Remote Sens Environ* **112**: 3341–3352.
- Hartmann, M., Grob, C., Tarran, G.A., Martin, A.P., Burkill, P.H., Scanlan, D.J., and Zubkov, M.V. (2012) Mixotrophic basis of Atlantic oligotrophic ecosystems. *Proc Natl Acad Sci U S A* **109**: 5756–5760.
- Hernando-Morales, V., Ameneiro, J., and Teira, E. (2017) Water mass mixing shapes bacterial biogeography in a

- highly hydrodynamic region of the Southern Ocean. *Environ Microbiol* **19**: 1017–1029.
- Herndl, G.J., Agogue, H., Baltar, F., Reinthaler, T., Sintes, E., and Varela, M.M. (2008) Regulation of aquatic microbial processes: the “microbial loop” of the sunlit surface waters and the dark ocean dissected. *Aquat Microb Ecol* **53**: 59–68.
- Hutchins, D.A., Walworth, N.G., Webb, E.A., Saito, M.A., Moran, D., McIlvin, M.R., et al. (2015) Irreversibly increased nitrogen fixation in *Trichodesmium* experimentally adapted to elevated carbon dioxide. *Nat Commun* **6**: 1–7.
- Ibarbalz, F.M., Henry, N., Brandão, M.C., Martini, S., Busseni, G., Byrne, H., et al. (2019) Global trends in marine plankton diversity across kingdoms of life. *Cell* **179**: 1084–1097.e21.
- Irwin, A.J., Finkel, Z.V., Schofield, O.M.E., and Falkowski, P. G. (2006) Scaling-up from nutrient physiology to the size-structure of phytoplankton communities. *J Plankton Res* **28**: 459–471.
- Kemp, W.M., and Mitsch, W.J. (1979) Turbulence and phytoplankton diversity: a general model of the “paradox of plankton”. *Ecol Model* **7**: 201–222.
- Kollmann, J., Meyer, S.T., Bateman, R., Conradi, T., Gossner, M.M., de Souza Mendonça, M., et al. (2016) Integrating ecosystem functions into restoration ecology—recent advances and future directions. *Restor Ecol* **24**: 722–730.
- Lea, D.J., Mirouze, I., Martin, M.J., King, R.R., Hines, A., Walters, D., and Thurlow, M. (2015) Assessing a new coupled data assimilation system based on the met office coupled atmosphere-land-ocean-sea ice model. *Mon Weather Rev* **143**: 4678–4694.
- Legendre, L. (1981) Hydrodynamic control of marine phytoplankton production: the paradox of stability. *Elsevier Oceanogr Ser* **32**: 191–207.
- Longhurst, A. (2007) Toward an ecological geography of the sea. In *Ecological Geography of the Sea*, 2nd ed: London, UK: Academic Press.
- Martiny, J.B.H., Bohannan, B.J.M., Brown, J.H., Kane, M., Krumins, J.A., Kuske, C.R., et al. (2006) Microbial biogeography: putting microorganisms on the map. *Nature* **4**: 102–112.
- Mayol, E., Jiménez, M.A., Herndl, G.J., Duarte, C.M., and Arrieta, J.M. (2014) Resolving the abundance and air-sea fluxes of airborne microorganisms in the North Atlantic Ocean. *Front Microbiol* **5**: 1–9.
- Milici, M., Tomasch, J., Wos-Oxley, M.L., Decelle, J., Jáuregui, R., Wang, H., et al. (2016) Bacterioplankton biogeography of the Atlantic Ocean: a case study of the distance-decay relationship. *Front Microbiol* **7**: 1–15.
- Mousing, E.A., Richardson, K., Bendtsen, J., Cetinić, I., and Perry, M.J. (2016) Evidence of small-scale spatial structuring of phytoplankton alpha- and beta-diversity in the open ocean. *J Ecol* **104**: 1682–1695.
- Nogales, B., Lanfranconi, M.P., Piña-Villalonga, J.M., and Bosch, R. (2011) Anthropogenic perturbations in marine microbial communities. *FEMS Microbiol Rev* **35**: 275–298.
- Oldham, C.E., Farrow, D.E., and Peiffer, S. (2013) A generalized Damköhler number for classifying material processing in hydrological systems. *Hydrol Earth Syst Sci* **17**: 1133–1148.
- Oliver, M.J., and Irwin, A.J. (2008) Objective global ocean biogeographic provinces. *Geophys Res Lett* **35**: 1–6.
- Olson, D.M., Dinerstein, E., Wikramanayake, E.D., Burgess, N.D., Powell, G.V.N., Underwood, E.C., et al. (2001) Terrestrial ecoregions of the world: a new map of life on earth. *Bioscience* **51**: 933–938.
- Powell, T.M., Richerson, P.J., Dillon, T.M., Agee, B.A., Dozier, B.J., Godden, D.A., and Myrup, L.O. (1975) Spatial scales of current speed and phytoplankton biomass fluctuations in Lake Tahoe. *Science* **189**: 1088–1090.
- Pruesse, E., Peplies, J., Glöckner, F.O., Editor, A., and Wren, J. (2012) SINA: accurate high-throughput multiple sequence alignment of ribosomal RNA genes. *Bioinformatics* **28**: 1823–1829.
- QGIS Development Team (2020). QGIS Geographic Information System. Open Source Geospatial Foundation Project. <http://qgis.osgeo.org>.
- Quast, C., Pruesse, E., Yilmaz, P., Gerken, J., Schweer, T., Glo, F.O., and Yarza, P. (2013) The SILVA ribosomal RNA gene database project: improved data processing and web-based tools. *Nucleic Acids Res* **41**: D590–D596.
- Raes, E.J., Bodrossy, L., Van De Kamp, J., Bissett, A., Ostrowski, M., and Brown, M.V. (2018) Oceanographic boundaries constrain microbial diversity gradients in the South Pacific Ocean. *Proc Natl Acad Sci U S A* **115**: E8266–E8275.
- Raes, J., Letunic, I., Yamada, T., Jensen, L.J., and Bork, P. (2011) Toward molecular trait-based ecology through integration of biogeochemical, geographical and metagenomic data. *Mol Syst Biol* **7**: 1–9.
- R Core Team (2020). *R: A language and environment for statistical computing*. Vienna: R Foundation for Statistical Computing. <https://www.R-project.org>
- Richter, D., Watteaux, R., Vannier, T., Leconte, J., Reygondeau, G., Maillet, N., et al. (2020) Genomic evidence for global ocean plankton biogeography shaped by large-scale current systems. *HAL Arch* **867739**: 1–38. <https://doi.org/10.1101/867739>
- RStudio Team (2021). *RStudio: Integrated Development Environment for R*. RStudio. Boston, MA: PBC. <http://www.rstudio.com>
- Santi, I., Tsiola, A., Dimitriou, P.D., Fodelianakis, S., Kasapidis, P., Papageorgiou, N., et al. (2019) Prokaryotic and eukaryotic microbial community responses to N and P nutrient addition in oligotrophic Mediterranean coastal waters: novel insights from DNA metabarcoding and network analysis. *Mar Environ Res* **150**: 104752.
- Seibold, S., Cadotte, M.W., Macivor, J.S., Thorn, S., and Müller, J. (2018) The necessity of multitrophic approaches in community ecology. *Trends Ecol Evol* **33**: 754–764.
- Seymour, J.R., Amin, S.A., Raina, J.B., and Stocker, R. (2017) Zooming in on the phycosphere: the ecological interface for phytoplankton-bacteria relationships. *Nat Microbiol* **2**: 17065.
- Sommeria-Klein, G., Watteaux, R., Iudicone, D., Bowler, C., and Morlon, H. (2021) Global drivers of eukaryotic plankton bioregionalization in the upper ocean. *Science* **374**: 594–599. <https://doi.org/10.1126/science.abb3717>
- Stec, K.F., Caputi, L., Buttigieg, P.L., D’Alelio, D., Ibarbalz, F.M., Sullivan, M.B., et al. (2017) Modelling

- plankton ecosystems in the meta-omics era. Are we ready? *Mar Genomics* **32**: 1–17.
- Steiner, C.F., and Leibold, M.A. (2004) Cyclic assembly trajectories and scale-dependent productivity – diversity relationships. *Ecol Soc Am* **85**: 107–113.
- Stoeck, T., Bass, D., Nebel, M., Christen, R., and Meredith, D. (2010) Multiple marker parallel tag environmental DNA sequencing reveals a highly complex eukaryotic community in marine anoxic water. *Mol Ecol* **19**: 21–31.
- Strass, V. (2018) The expedition PS113 of the research vessel POLARSTERN to the Atlantic Ocean in 2018. *Berichte Polar Meeresforsch* **714**: 66.
- Sunagawa, S., Coelho, L.P., Chaffron, S., Kultima, J.R., Labadie, K., Salazar, G., *et al.* (2015) Structure and function of the global ocean microbiome. *Science* **348**: 1261359.
- Taylor, B.B., Torrecilla, E., Bernhardt, A., Taylor, M.H., Peeken, I., Röttgers, R., *et al.* (2011) Bio-optical provinces in the eastern Atlantic Ocean and their biogeographical relevance. *Biogeosciences* **8**: 3609–3629.
- Teira, E., Logares, R., Gutiérrez-Barral, A., Ferrera, I., Varela, M.M., Morán, X.A.G., and Gasol, J.M. (2019) Impact of grazing, resource availability and light on prokaryotic growth and diversity in the oligotrophic surface global ocean. *Environ Microbiol* **21**: 1482–1496.
- Thompson, L.R., Field, C., Romanuk, T., Kamanda Ngugi, D., Siam, R., El Dorry, H., and Stingl, U. (2013) Patterns of ecological specialization among microbial populations in the Red Sea and diverse oligotrophic marine environments. *Ecol Evol* **3**: 1780–1797.
- Troussellier, M., Escalas, A., Bouvier, T., and Mouillot, D. (2017) Sustaining rare marine microorganisms: macroorganisms as repositories and dispersal agents of microbial diversity. *Front Microbiol* **8**: 1–17.
- Vallina, S.M., Follows, M.J., Dutkiewicz, S., Montoya, J.M., Cermeno, P., and Loreau, M. (2014) Global relationship between phytoplankton diversity and productivity in the ocean. *Nat Commun* **5**: 1–10.
- von Appen, W.-J., Strass, V.H., Bracher, A., Xi, H., Hörstmann, C., Iversen, M.H., and Waite, A.M. (2020) High-resolution physical–biogeochemical structure of a filament and an eddy of upwelled water off northwest Africa. *Ocean Sci* **16**: 253–270.
- Woodward, F.I. (1987) *Climate and Plant Distribution*. Cambridge, UK: Cambridge University Press.
- Woodward, F.I., Lomas, M.R., and Kelly, C.K. (2004) Global climate and the distribution of plant biomes. *Philos Trans R Soc B Biol Sci* **359**: 1465–1476.
- Yilmaz, P., Kottmann, R., Field, D., Knight, R., Cole, J.R., Amaral-zettler, L., *et al.* (2011) Perspective minimum information about a marker gene sequence (MIMARKS) and minimum information about any (x) sequence (MIXS) specifications. *Nature* **29**: 415–420.
- Zeebe, R., and Wolf-Gladrow, D. (2001) *CO<sub>2</sub> in Seawater: Equilibrium, Kinetics, Isotopes*, Vol. **65**. Houston, TX: Gulf Professional Publishing.
- Zhou, J., Deng, Y., Zhang, P., Xue, K., Liang, Y., Van Nostrand, J.D., *et al.* (2014) Stochasticity, succession, and environmental perturbations in a fluidic ecosystem. *Proc Natl Acad Sci U S A* **111**: E836–E845.

## Supporting Information

Additional Supporting Information may be found in the online version of this article at the publisher's web-site:

**Appendix S1:** Supplementary Information.